Electronic Transactions on Numerical Analysis.
Volume 33, pp. 105-125, 2009.
Copyright © 2009, Kent State University.
ISSN 1068-9613.

ETNA
Kent State University
http://etna.math.kent.edu

NUMERICAL LINEAR ALGEBRA FOR NONLINEAR MICROWAVE IMAGING*

FABIO DI BENEDETTO†, CLAUDIO ESTATICO‡, JAMES G. NAGY§, AND MATTEO PASTORINO¶

Abstract. A nonlinear inverse scattering problem arising in microwave imaging is analyzed and numerically solved. In particular, the dielectric properties of an inhomogeneous object (i.e., the image to restore) are retrieved by means of its scattered microwave electromagnetic field (i.e., the input data) in a tomographic arrangement. From a theoretical point of view, the model gives rise to a nonlinear integral equation, which is solved by a deterministic and regularizing inexact Gauss-Newton method. At each step of the method, matrix strategies of numerical linear algebra are considered in order to reduce the computational (time and memory) load for solving the obtained large and structured linear systems. These strategies involve block decompositions, splitting and regularization, and super-resolution techniques. Some numerical results are given where the proposed algorithm is applied to recover high resolution images of the scatterers.

Key words. inverse scattering, microwave imaging, inexact-Newton methods, block decomposition, regularization.

AMS subject classifications. 65F22, 65R32, 45Q05, 78A46

1. Introduction.

Nonlinear inverse problems, which arise in many important applications, present significant mathematical and computational challenges [10]. For example, it is often difficult to determine existence and uniqueness of an analytical solution in a theoretical setting. But even in cases where these properties are known, and a particular solution is sought, solving the problem in a discrete setting may still be very difficult. Indeed, numerically solving a nonlinear inverse problem generally requires solving a computationally expensive optimization problem involving very large-scale linear systems. In addition, because the underlying continuous problem is ill-posed, solutions are typically very sensitive to noise in the measured data. Thus, special considerations are needed in developing and implementing algorithms to solve these problems.

In this paper we develop an efficient approach to compute approximate solutions of a nonlinear image reconstruction problem from inverse scattering [7, 20]. Specifically, we consider the problem of reconstructing the internal dielectric properties of an object based on knowledge of the external scattered electric field, which is generated by the interaction between the object and a known incident electromagnetic microwave. Applications that use this imaging technique range from civil and industrial engineering (nondestructive testing and material characterization) to detection of buried objects and medical diagnostics.

In order to restore the unknown object, the external scattered electric field must be evaluated from known incident electromagnetic waves. The relationship between the scattered electric field and the incident electromagnetic waves is modeled by an integral equation. Because the problem is highly underdetermined, a single incident electromagnetic wave is insufficient to reconstruct an accurate approximation of the object. It is therefore necessary

* Received March 8, 2008. Accepted October 24, 2008. Published online on October 22, 2009. Recommended by K. Jbilou. The work of F. Di Benedetto and C. Estatico was partially supported by MIUR, grant number 2006017542. The work by J. Nagy was supported by the NSF under grant DMS-05-11454.

†Dipartimento di Matematica, Università degli Studi di Genova, Via Dodecaneso 35, 16146 Genova, Italy (dibenede@dima.unige.it)

‡Dipartimento di Matematica e Informatica, Università degli Studi di Cagliari, Via Ospedale 72, 09124 Cagliari, Italy (estatico@unica.it)

§Mathematics & Computer Science Department, Emory University, Atlanta, GA 30322, USA (nagy@mathcs.emory.edu)

¶Dipartimento di Ingegneria Biofisica ed Elettronica, Università degli Studi di Genova, via all'Opera Pia 11a, 16145 Genoa, Italy (pastorino@dibe.unige.it)

ETNA
Kent State University
http://etna.math.kent.edu

to increase information by using several different incident electromagnetic waves. Another complication is that the scattered electric field inside the object also needs to be approximated, since it is required to invert the above integral operator. In some basic cases, a simplified approximation of the internal scattered field can be used; see the Born approximations for weak scatterers in [7]. We, however, do not use this assumption, but instead consider the internal scattered field as an additional unknown to recover. Our proposed scheme is therefore very general, and can be used, for example, in applications when strong scatterers are introduced.

The approach we use to solve the resulting nonlinear image reconstruction problem is based on Newton linearization techniques to deal with the nonlinearity, and regularization techniques to deal with the ill-posedness [9]. The focus of this paper is on the use of numerical linear algebra tools to exploit structure and sparsity of the large-scale linear systems that need to be solved in the optimization algorithm. To further reduce the complexity of the problem, we propose to recover first a number of low resolution approximations of the output object using a coarse discretization and, after that, to reconstruct a single output image with higher resolution. The low resolution images will be obtained in such a way that they represent reconstructions of the object after it has been shifted by subpixel displacements. Super-resolution methods [3, 6, 8, 11, 17, 19, 21] will then be used to fuse the different information available in the low resolution images to obtain the high resolution image.

To reconstruct each of the low resolution images, we propose to use a regularizing three-level iterative algorithm, where a Gauss-Newton linearizing scheme (the first level, or outermost iterative method) is inexactly solved at each iteration by an iterative block splitting method (this is the second level, or the first inner iteration). The block iteration involves a sequence of smaller linear systems, which are then solved by a basic (e.g., Landweber) iterative regularization method (this is the third level, or the innermost iteration).

The paper is outlined as follows. In Section 2 we describe the mathematical model of the inverse scattering problem from microwave imaging and the structure of the block matrix arising in our linearization approach. The three-level iterative algorithm and appropriate numerical linear algebra tools to solve the resulting nonlinear optimization problem, and to do the super-resolution post-processing, are developed in Section 3. Numerical results are reported in Section 4.

2. Mathematical formulation. Although the mathematical model for the inverse scattering problem can be introduced in a general three-dimensional setting, to simplify notation, we focus on the two-dimensional case. From a theoretical point of view, the mathematical model is related to the tomographic configuration for retrieving the cross section of an "infinite" cylindrical object.

2.1. The mathematical model. Let us consider a cylindrical scatterer embedded in a linear and homogeneous medium (the background), whose cross section is strictly contained in a known, bounded, and simply connected plane of investigation $\Omega \subset \mathbb{R}^2$. The dielectric properties of Ω are described by the inhomogeneous contrast function $\chi : \Omega \longrightarrow \mathbb{C}$, $\chi(r) = \epsilon(r)/\epsilon_b - 1$, where the relative refractive index $\epsilon(r)/\epsilon_b$ is the ratio between the dielectric permittivity $\epsilon(r)$ at the point $r \in \Omega$ (the position coordinate), and the constant dielectric permittivity ϵ_b of the background. Since the cross section of the scatterer is contained in Ω, the contrast function χ has compact support, which we assume is endowed with Lipschitz continuous smooth boundary.

A known incident field u^i interacts with the scatterer, leading to a total field u on $\mathbb{R}^2$ which is the sum of the incident field u^i and the scattered field u^s; that is, $u = u^i + u^s$. The *direct* (or *forward*) scattering problem is to compute the total field u from the dielectric properties of the domain Ω. The *inverse* scattering problem is to retrieve the contrast function χ, from measurements of the total field u in a region of observation $\Omega^{(M)}$ (usually disjoint from Ω). In addition, the total electric field u in the region Ω is unknown, since that region is inaccessible to measurements.

Assuming no magnetic media are involved, the classical differential model for the direct scattering problem with Sommerfeld radiation condition at infinity [7] has the following equivalent Lippmann-Schwinger integral formulation

$$u(r) - \int_{\Omega} G(r,\tilde{r})\, u(\tilde{r})\, \chi(\tilde{r})\, d\tilde{r} = u^i(r)\,, \qquad \forall r \in \mathbb{R}^2, \tag{2.1}$$

where $G(r,\tilde{r}) = -k_b^2 \frac{j}{4} H_0^{(2)}(k_b\|r-\tilde{r}\|)$ is the Green's function for the two-dimensional Helmholtz equation, $H_0^{(2)}$ is a zeroth order, second kind Hankel function, $j^2 = -1$, and $k_b = \omega\sqrt{\epsilon_b \mu_0}$ is the background wave number for the magnetic permeability of the vacuum μ_0, with angular frequency ω. We remark that the integral operator on the left side is nonlinear with respect to χ, since the total field u, generated by the interaction between the scatterer and the incident field, depends on χ.

Concerning the direct problem with fixed scattering potential χ, if the incident field u^i is a plane electromagnetic wave $u^i(x) = \exp(-jk_b x \cdot d)$ on Ω, where $d \in S^2 = \{x \in \mathbb{R}^2 : \|x\| = 1\}$ is the incident direction, then a solution $u \in L^2(\mathbb{R}^2)$ satisfying (2.1) exists and is unique for all wavenumbers $k_b > 0$ and all incident directions $d \in S^2$ [7, 18].

For the inverse scattering problem, a solution χ is unique whenever it exists, but the problem is severely ill-posed; see [7] for a comprehensive discussion of the topic. However, the integral formulation (2.1) cannot be used straightforwardly to retrieve the scattering potential χ, since the total field u can only be measured in the observation domain $\Omega^{(M)}$. We therefore must consider its restriction on $\Omega^{(M)}$

$$\int_{\Omega} G(r,\tilde{r})\, u(\tilde{r})\, \chi(\tilde{r})\, d\tilde{r} = u^s(r)\,, \qquad \forall r \in \Omega^{(M)}, \tag{2.2}$$

where the scattered field $u^s = u - u^i$ on $\Omega^{(M)}$ represents the data we collect for the inverse problem.

Recall that, in the above integrand, the total electric field u in the region Ω is unknown. For this reason, together with (2.2), we consider in our scheme the following integral Fredholm operator of the second type

$$u(r) - \int_{\Omega} G(r,\tilde{r})\, u(\tilde{r})\, \chi(\tilde{r})\, d\tilde{r} = u^i(r)\,, \qquad \forall r \in \Omega, \tag{2.3}$$

which represents the implicit relationship between the unknown total and the known incident electric fields. The idea is then to use the coupled integral equations (2.2) and (2.3) to simultaneously compute χ and u on Ω, by means of a fixed point iterative scheme.

Unfortunately, the pair of nonlinear integral equations (2.2)–(2.3) is not enough to solve the inverse problem. Indeed, the classical theory of inverse scattering requires that the scattered data be known for all wavenumbers $k_b > 0$ and all incident directions $d \in S^2$ in order to solve the inverse problem. In a real setting, we can use a finite set of P different configurations of the source (incident field), which allows us to collect more information about the scattered field in different radiation conditions, and, in the end, more information about the scatter. The different source configurations are attained by varying

(i) the position of the whole apparatus, including both the emitting antenna and the co-moving receiving detectors, and
(ii) the frequency of the incident microwaves.

ETNA
Kent State University
http://etna.math.kent.edu

Let u_p^i denote the incident electric field produced by the pth source, and let u_p be the resulting total electric field measured in a region $\Omega_p^{(M)}$, which is disjoint from Ω. The aim of the inverse scattering problem is thus to retrieve a good approximation of the contrast function χ on Ω, given knowledge of all the electric fields $u_p^s \in L^2(\Omega_p^{(M)})\,,\ p = 1, \ldots, P$.

The integral equations (2.2) and (2.3) can be regarded as a system where the unknowns are χ and $\{u_p\}_{p=1,\ldots,P}$ in Ω, while the known terms are $\{u_p^i\}_{p=1,\ldots,P}$ in Ω (recall that the incident fields are known everywhere) and the scattered electric fields $\{u_p^s\}_{p=1,\ldots,P}$, with u_p^s in $\Omega_p^{(M)}$, for $p = 1, \ldots, P$.

By introducing the nonlinear operator $A : \prod_{p=1}^{P+1} L^2(\Omega) \rightarrow (\prod_{p=1}^{P} L^2(\Omega_p^{(M)})) \times (\prod_{p=1}^{P} L^2(\Omega))$

$$A(u_1, \ldots, u_P,\, \chi)(r) = \begin{bmatrix} \int_\Omega G(r,\tilde r)\, u_1(\tilde r)\, \chi(\tilde r)\, d\tilde r \\ \vdots \\ \int_\Omega G(r,\tilde r)\, u_P(\tilde r)\, \chi(\tilde r)\, d\tilde r \\ u_1(r) - \int_\Omega G(r,\tilde r)\, u_1(\tilde r)\, \chi(\tilde r)\, d\tilde r \\ \vdots \\ u_P(r) - \int_\Omega G(r,\tilde r)\, u_P(\tilde r)\, \chi(\tilde r)\, d\tilde r \end{bmatrix}, \tag{2.4}$$

and the known vector $b \in (\prod_{p=1}^{P} L^2(\Omega_p^{(M)})) \times (\prod_{p=1}^{P} L^2(\Omega))$

$$b = \left(u_1^s, \ldots, u_P^s, u_1^i, \ldots, u_P^i\right)^T, \tag{2.5}$$

the inverse scattering problem can be formally stated as the following functional equation: find $\chi \in L^2(\Omega)$ and $u_p \in L^2(\Omega)\,,\ p = 1, \ldots, P$, such that

$$A(u_1, \ldots, u_P,\, \chi) = b. \tag{2.6}$$

As is well known, the nonlinear inverse scattering problem is ill-posed, and a regularization strategy is needed to stabilize the inversion process. In this paper, we use a suitably regularized inexact-Newton iterative algorithm.

2.2. The Fréchet Derivative for the Newton schemes. Let the Hilbert spaces $X = \prod_{p=1}^{P+1} L^2(\Omega)$ and $Y = (\prod_{p=1}^{P} L^2(\Omega_p^{(M)})) \times (\prod_{p=1}^{P} L^2(\Omega))$ denote the domain and codomain of the operator A defined in (2.4). The Newton methods require the computation of the Fréchet derivative of A. We recall that the Fréchet derivative of the operator A at the point $x = (u_1, \ldots, u_P,\, \chi) \in X$ is the linear operator $A'_x : X \longrightarrow Y$ such that

$$A(x + h) = A(x) + A'_x h + o(\|h\|). \tag{2.7}$$

Concerning the existence of such a derivative, since the integral formulation (2.1) is Fréchet differentiable [16], both (2.2) and (2.3) are Fréchet differentiable; therefore the operator A is Fréchet differentiable, too.

By using this notation, the classical Newton scheme for the nonlinear equation $A(x) = b$ is formally the following: let $x_0 \in X$ be an appropriate initial guess, and compute, for $k = 0, 1, 2, \ldots$, the iterative steps $x_{k+1} = x_k - (A'_{x_k})^{-1}(A(x_k) - b)$, where the Fréchet derivative A'_{x_k} is required to be invertible. Since in inverse problems the Fréchet derivative is usually a non-invertible and ill-posed operator, the previous simple classical scheme cannot be used in real applications. In practice, some regularization techniques must be introduced in order to regularize the solution of each Newton step. This way, the iterative scheme becomes the following, namely the inexact Gauss-Newton method,

$$x_{k+1} = x_k - \phi(k, A_{x_k}'^* A_{x_k}')\, A_{x_k}'^*(A(x_k) - b), \tag{2.8}$$

where $*$ denotes the adjoint operator, $\phi(k,\lambda) : \mathbb{N} \times [0, +\infty) \longrightarrow \mathbb{R}$ is a piecewise continuous function, and the evaluation of ϕ on the operator in (2.8) has the classical meaning in the context of spectral theory [9]. Formally, the role of ϕ consists of regularizing the computation of the least squares solution $(A_{x_k}'^* A_{x_k}')^{-1} A_{x_k}'^*(A(x_k) - b)$ of the Newton step.

The simplest method belonging to the general scheme (2.8) is the Landweber algorithm for nonlinear problems, where the regularizing scheme ϕ is a constant function. In particular, $\phi(k,\lambda) = \tau > 0$, where τ depends on the spectral norm of $A_x'^* A_x'$ in a neighborhood of the solution, leading to $\phi(k, A_{x_k}'^* A_{x_k}') = \tau A_{x_k}'^* A_{x_k}'$ [14]. The widely used Levenberg-Marquardt method belongs to the class (2.8), too, since here $\phi(k,\lambda) = (\lambda + \mu_k)^{-1}$, where $\mu_k > 0$ is a regularization parameter, leading to $\phi(k, A_{x_k}'^* A_{x_k}') = (A_{x_k}'^* A_{x_k}' + \mu_k I)^{-1}$ (notice that the method is Gauss-Newton with Tikhonov regularization on the linearization). Another instance of (2.8) is the Gauss-Newton method with truncated singular value decomposition, where $\phi(k,\lambda) = \lambda^{-1}$, for $\lambda \geq T_k$, and $\phi(k,\lambda) = 0$ otherwise; in this case the regularization parameter is the truncation threshold, T_k.

An important set of methods of type (2.8) is the class of Gauss-Newton methods with iterative inner regularization [23], where the function ϕ is evaluated by means of an iterative formula. This is the case of the inexact Gauss-Newton method when the inner regularization is performed by means of d Landweber iterations. In this case, the regularizing scheme ϕ is a polynomial approximation of the inverse function. In particular, $\phi(k,\lambda) = P_d(\lambda)$, where $d = d(k) \in \mathbb{N}$ and P_d is the d-degree polynomial $P_d(\lambda) = \tau \sum_{i=0}^{d} (1 - \tau\lambda)^i = \frac{1-(1-\tau\lambda)^{d+1}}{\lambda}$ [5].

The purpose of the parameter $\tau > 0$ is to control and to accelerate the convergence of the iterates along the different components. In particular, consider the eigenspace related to a fixed eigenvalue λ of $A_{x_k}'^* A_{x_k}'$: after the application of the regularizing operator $\phi(k, A_{x_k}'^* A_{x_k}')$, the vector $A_{x_k}'^*(A(x_k) - b)$ is multiplied along that component by $P_d(\lambda)$. Thus, in the computation of the (generalized) solution δ of $A_{x_k}'^* A_{x_k}' \delta = A_{x_k}'^*(A(x_k) - b)$, the relative error in the same component is

$$\left| \left(\frac{1-(1-\tau\lambda)^{d+1}}{\lambda} - \frac{1}{\lambda} \right) \Big/ \frac{1}{\lambda} \right| = |1 - \tau\lambda|^{d+1};$$

for a detailed discussion, see [5, Equations (2.10)–(2.11)]). This means that the convergence of the iterations toward the solution δ is slow along the components for which the value of λ is close to 0 or $2\tau^{-1}$, whereas it is the fastest one when λ is close to τ^{-1}. Therefore, the convergence is always slow in the space where λ is small, which is usually the space corrupted by noise in inverse problems, but an appropriate choice of τ enables us to "select" the most important subspace of components to be first resolved in the Landweber iterative resolution process. For instance, the simple choice $\tau = \|A_{x_k}'^* A_{x_k}'\|_2^{-1}$ provides the fast convergence of the solution in the subspace related to the largest eigenvalues of $A_{x_k}'^* A_{x_k}'$, which usually contains much information and is less sensitive to the noise on the data.

From a computational point of view, since $P_d(\lambda) = P_{d-1}(\lambda) + \tau(1 - \lambda P_{d-1}(\lambda))$, the evaluation of $\phi(k, A_{x_k}'^* A_{x_k}')\, A_{x_k}'^*(A(x_k) - b)$ in the second term of (2.8) is efficiently computed by the following iterative procedure:

$$f_0 = 0, \quad f_{s+1} = f_s + \tau A_{x_k}'^*((A(x_k) - b) - A_{x_k}' f_s), \quad s = 0, 1, \ldots, d.$$

For nonlinear inverse problems it is very important that solutions of the inner linear system not be corrupted by noise; it is better to compute a solution that is over-regularized than

ETNA
Kent State University
http://etna.math.kent.edu

one that is under-regularized. Iterative methods that converge slowly, such as Landweber, have better noise filtering properties and do not require as precise a stopping criteria as iterative methods that converge very quickly, such as conjugate gradients [13]. It is for this reason that Landweber is often chosen to solve the inner linear systems that arise from nonlinear inverse problems. We remark that a higher degree d of the polynomial $P_d(\lambda)$ results in a better approximation of the inverse function λ^{-1}, and thus reduces the regularization effects of the Landweber inner iteration. In this respect, it is interesting to notice that if $d = 0$, this method corresponds to the classical Landweber algorithm for nonlinear problems. In this case, the regularizing scheme ϕ is a constant function, which can be considered as the slowest and most regularizing algorithm among all the Gauss-Newton methods with Landweber inner regularization.

By means of simple algebraic computations based on its definition (2.7), the computation of the Fréchet derivative of the operator A at the point $x = (u_1, \ldots, u_P, \chi)$ gives rise to the following sparse and structured matrix

$$A'_x = \begin{bmatrix} A^{(M)}_{\chi,1} & 0 & \ldots & 0 & A^{(M)}_{u,1} \\ 0 & A^{(M)}_{\chi,2} & \ddots & \vdots & A^{(M)}_{u,2} \\ \vdots & \ddots & \ddots & 0 & \vdots \\ 0 & \ddots & \ddots & A^{(M)}_{\chi,P} & A^{(M)}_{u,P} \\ I - A_\chi & \ddots & \ddots & 0 & -A_{u,1} \\ 0 & I - A_\chi & \ddots & \vdots & -A_{u,2} \\ \vdots & \ddots & \ddots & 0 & \vdots \\ 0 & \ldots & 0 & I - A_\chi & -A_{u,P} \end{bmatrix}, \tag{2.9}$$

where $\{A^{(M)}_{\chi,p}\}_{p=1,\ldots,P}$, $\{A^{(M)}_{u,p}\}_{p=1,\ldots,P}$, $\{A_{u,p}\}_{p=1,\ldots,P}$, and A_χ are the following linear operators:

$$\begin{aligned} A^{(M)}_{\chi,p} h(r) &= \int_\Omega G(r,\tilde r)\, h(\tilde r)\, \chi(\tilde r)\, d\tilde r, && r \in \Omega^{(M)}_p, \\ A^{(M)}_{u,p} h(r) &= \int_\Omega G(r,\tilde r)\, u_p(\tilde r)\, h(\tilde r)\, d\tilde r, && r \in \Omega^{(M)}_p, \\ A_{u,p} h(r) &= \int_\Omega G(r,\tilde r)\, u_p(\tilde r)\, h(\tilde r)\, d\tilde r, && r \in \Omega, \\ A_\chi h(r) &= \int_\Omega G(r,\tilde r)\, h(\tilde r)\, \chi(\tilde r)\, d\tilde r, && r \in \Omega. \end{aligned}$$

The notation of the blocks of the Fréchet derivative A'_x recalls the dependence on the parameters in the associated integral kernels.

As an example of computation, for the partial derivatives in the first row of A'_x we have to linearize the first component of the operator A in (2.4) by considering an argument $x + h$, where $x = (u_1, \ldots, u_P, \chi)$ and $h = (h_1, h_2, \ldots, h_P, h_\chi)$:

$$\begin{aligned} &\int_\Omega G(r,\tilde r)\, (u_1 + h_1)(\tilde r)\, (\chi + h_\chi)(\tilde r)\, d\tilde r - \int_\Omega G(r,\tilde r)\, u_1(\tilde r)\, \chi(\tilde r)\, d\tilde r \\ = &\int_\Omega G(r,\tilde r)\, h_1(\tilde r)\, \chi(\tilde r)\, d\tilde r + \int_\Omega G(r,\tilde r)\, u_1(\tilde r)\, h_\chi(\tilde r)\, d\tilde r + \int_\Omega G(r,\tilde r)\, h_1(\tilde r)\, h_\chi(\tilde r)\, d\tilde r, \end{aligned}$$

ETNA
Kent State University
http://etna.math.kent.edu

for $r \in \Omega_1^{(M)}$. Since $\int_\Omega G(r,\tilde r)\, h_1(\tilde r)\, h_\chi(\tilde r)\, d\tilde r = O(\|h\|^2)$, the first two integral operators on the right-hand side represent the Fréchet derivative of the mentioned component, applied to the variables contained in h. Therefore there is no dependence on $h_2, \ldots, h_P$ whereas these two terms are respectively the matrix blocks $A_{\chi,1}^{(M)}$ (derivative with respect to u_1) and $A_{u,1}^{(M)}$ (derivative with respect to χ) in the first row of (2.9) [4].

2.3. Computation of the operators. It is important to notice that in our iterative solving scheme, which is based on the inexact-Newton method (2.8) and on the linearization (2.9), it is required to compute many integrals involving the Green's function G. These integrals arise in the forward operator A and in the Fréchet derivative A'_x, and all are of the form

$$I(r) = \int_\Omega G(r,\tilde r)\, g_1(\tilde r)\, g_2(\tilde r)\, d\tilde r,$$

where both the functions g_1 and g_2 are known. In the computation of electromagnetic fields for applications in many areas as well as in our algorithm, these integrals are well approximated by using the so-called moment method [15]. In particular, each integral $I(r)$ is approximated by considering a partitioning $\{\Omega_s\}_{s=1,\ldots,S}$ of the integration domain Ω (i.e., $\Omega = \cup_{s=1}^S \Omega_s$ and $\Omega_{s_1} \cap \Omega_{s_2} = \emptyset$ if $s_1 \neq s_2$) so that

$$I(r) = \int_\Omega G(r,\tilde r)\, g_1(\tilde r)\, g_2(\tilde r)\, d\tilde r = \sum_{s=1}^S \int_{\Omega_s} G(r,\tilde r)\, g_1(\tilde r)\, g_2(\tilde r)\, d\tilde r.$$

If a partitioning is sufficiently small, then

$$I(r) \approx \sum_{s=1}^S g_1(r_s)\, g_2(r_s) \int_{\Omega_s} G(r,\tilde r)\, d\tilde r,$$

where r_s is the barycenter of Ω_s. As a result, the computation of the integral $I(r)$ is reduced to the computation of all the integrals $\int_{\Omega_s} G(r,\tilde r)\, d\tilde r$, which are independent of both the functions u and χ, and thus can be computed once for all the iterations. In scattering imaging applications, a very useful analytical expression for these integrals is obtained by approximating each subdomain Ω_s by a circle C_s of equivalent area. Indeed, in this case the integral of the Green's function on a circle C_s is given by the following explicit formula [22]:

$$\int_{\Omega_s} G(r,\tilde r)\, d\tilde r \approx \int_{C_s} G(r,\tilde r)\, d\tilde r = k_b^2 \frac{j}{4} \pi d_s J_1(k_b d_s) H_0^{(2)}(k_b \|r - r_s\|)$$

(see the notation of (2.1)), where J_1 is the first order Bessel function of first kind, $d_s = \sqrt{\Delta\Omega_s/\pi}$ is the radius of the equivalent circle, and $\Delta\Omega_s$ the area of Ω_s. In our scheme, each domain Ω_s corresponds to a single (rectangular) discretization region. Thus, if $r = r_m$, where r_m is again the barycenter of the region Ω_m, we approximate all integrals in our algorithm by the moment method as

$$I(r_m) \approx \sum_{s=1}^S a_{m,s} g_1(r_s)\, g_2(r_s),$$

where the coefficients $a_{m,s} = k_b^2 \frac{j}{4} \pi d_s J_1(k_b d_s) H_0^{(2)}(k_b \|r_m - r_s\|)$ can be considered as the elements of a fixed matrix for the computation of each integral $I(r_m)$, for $m = 1, \ldots, S$. Notice that the above matrix has a scaled Toeplitz structure.

3. Numerical linear algebra tools for the Newton schemes. Newton methods require the computation of (a regularized approximation of) several linear equations involving the derivatives A'_x for $x \in X$. In a real setting, the discretization of the inverse scattering model leads to matrices A'_x whose dimensions are extremely large in general. Indeed, the discretization of the model consists of

- $n \times n$ pixels for the investigation domain Ω,
- m pointwise receiving detectors on each observation domain $\Omega_p^{(M)}$ for each source $p = 1, \dots, P$,
- $P = R \cdot F$ different sources of the incident field, where R is the number of rotations of the apparatus (the so-called views), and F is the number of frequencies of the incident microwave (the so-called illuminations) for each view.

Having introduced these constants, it is simple to check that any block $A_{\chi,p}^{(M)}$ is an $m \times n^2$ matrix, A_χ is $n^2 \times n^2$, any $A_{u,p}^{(M)}$ is $m \times n^2$, and any $A_{u,p}$ is $n^2 \times n^2$, so that the total size of the matrix A'_x is

$$(Pm + Pn^2) \times (Pn^2 + n^2) = P(m + n^2) \times (P + 1)n^2.$$

For instance, real data collected for the database of the Institut Fresnel of Marseille [1] comes from a device with $m = 241$ detectors on a circular observation domain $\Omega_p^{(M)}$ with a radius of about 1.5 meters, with $R = 18$ views and $F = 9$ different illuminations. In this setup, an $n \times n = 64 \times 64$ discretization of Ω gives rise to a matrix A'_x of about $7.0 \cdot 10^5 \times 6.7 \cdot 10^5$ elements. The same setting, with the larger discretization $n \times n = 1024 \times 1024$, gives a size for A'_x of about $1.7 \cdot 10^8 \times 1.7 \cdot 10^8$ elements!

It is essential to use advanced numerical linear algebra tools to reduce the computational complexity of reconstruction algorithms involving these large-scale linear systems. This goal can be reached by exploiting two peculiarities of the problem: (i) the sparsity and the block structure arising at the first level, and (ii) the structure arising in the individual blocks. In this paper we focus on the first approach.

3.1. Exploiting sparsity. Each inexact Newton step (2.8) involves the computation of the normal equation system matrix $E = A_x'^* A'_x$. It is simple to show that the normal equation system matrix E has the following block-arrow structure

$$E = A_x'^* A'_x = \begin{bmatrix} M_1 & & & & V_1 \\ & M_2 & & & V_2 \\ & & \ddots & & \vdots \\ & & & M_P & V_P \\ V_1^* & V_2^* & \dots & V_P^* & C \end{bmatrix}, \tag{3.1}$$

where each block has size $n^2 \times n^2$ and is the sum of products of structured matrix blocks of A'_x, since

$$\begin{aligned} M_p &= A_{\chi,p}^{(M)^*} A_{\chi,p}^{(M)} + (I - A_\chi)^*(I - A_\chi), \\ V_p &= A_{\chi,p}^{(M)^*} A_{u,p}^{(M)} + (A_\chi^* - I)A_{u,p}, \\ C &= \sum_{p=1}^{P} A_{u,p}^{(M)^*} A_{u,p}^{(M)} + \sum_{p=1}^{P} A_{u,p}^* A_{u,p}. \end{aligned}$$

The simple block-arrow structure of the normal equation system matrix E can be exploited in order to obtain solving schemes with low computational complexity. In the following subsections, we describe two approaches: a direct solver and a splitting iterative solver.

ETNA
Kent State University
http://etna.math.kent.edu

3.1.1. Block Cholesky Factorization. As already mentioned, inexact Newton schemes (2.8) for nonlinear functional equations arising in inverse problems usually require regularization at every linearized step. As a basic example, we consider the Tikhonov regularization method, where $\phi(k,\lambda) = 1/(\lambda+\mu)$ and $\mu = \mu(k) > 0$ is the regularization parameter that depends on the iteration index k. By considering the residual $r = b - A(x)$, each iteration of (2.8) with Tikhonov regularization can be written as $\tilde{x} = x + \tilde{h}$, where $\tilde{h}$ is the solution of the block-arrow linear system

$$\tilde{E}\tilde{h} = \tilde{b}, \tag{3.2}$$

where $\tilde{E} = E + \mu I = A_x'^* A_x' + \mu I$ and $\tilde{b} = A_x'^* r$.

In the case of symmetric positive definite block-arrow matrices, the Cholesky variant of LU factorization is very convenient. Indeed, since Cholesky factorization can be carried through without any need for pivoting or scaling, it does not give rise to any fill-in and it is numerically stable [12]. The result is that each Cholesky factor inherits the same arrow structure in its lower triangular part. By exploiting the block-arrow structure of $\tilde{E}$, Cholesky decomposition at the block level gives

$$\tilde{E} = LL^*,$$

with

$$L = \begin{bmatrix} L_1 & & & & \\ & L_2 & & & \\ & & \ddots & & \\ & & & L_P & \\ \hat{L}_1 & \hat{L}_2 & \dots & \hat{L}_P & \hat{L}_0 \end{bmatrix}. \tag{3.3}$$

Here the blocks of L are defined as follows:

- L_p is the Cholesky factor of the symmetric positive definite diagonal block $\tilde{M}_p = M_p + \mu I$; that is, $\tilde{M}_p = L_p L_p^*$ for $p = 1, \dots, P$.
- $\hat{L}_p = V_p L_p^{-*}$ is a full matrix, for $p = 1, \dots, P$.
- $\hat{L}_0$ is the Cholesky factor of the symmetric positive definite matrix $\tilde{C} - \sum_{p=1}^{P} \hat{L}_p \hat{L}_p^*$; that is, $\tilde{C} - \sum_{p=1}^{P} \hat{L}_p \hat{L}_p^* = \hat{L}_0 \hat{L}_0^*$, where $\tilde{C} = C + \mu I$.

Summarizing, thanks to the block-arrow structure of A_x', the Cholesky decomposition of the normal equation system matrix $\tilde{E}$ is computed efficiently by means of $P+1$ simple Cholesky decompositions at the inner block level only and P triangular inversions and matrix multiplications for computing each $\hat{L}_p$. The solution $\tilde{h}$ of the system (3.2) is then computed by forward and backward block substitutions, according to the following scheme:

- $v_p = L_p^{-1} b_p$, for $p = 1, \dots, P$,
- $v_\chi = \hat{L}_0^{-1}(b_\chi - \sum_{p=1}^{P} \hat{L}_p v_p)$,
- $h_\chi = \hat{L}_0^{-*} v_\chi$,
- $h_p = L_p^{-*}(v_p - \hat{L}_p^* h_\chi)$, for $p = 1, \dots, P$,

where $\tilde{b} = \big(b_1, b_2, \dots, b_P, b_\chi\big)^T$ and $\tilde{h} = \big(h_1, h_2, \dots, h_P, h_\chi\big)^T$. The overall cost of computing $\tilde{h}$ in this way is $(8P+1)n^3/6 + O(Pn^2)$ multiplicative operations.

3.1.2. Block iterative splitting methods. In the previous subsection, each linear system of the inexact Newton steps (2.8) with Tikhonov regularization is solved by a direct method based on the Cholesky block decomposition (3.3). In this subsection, we analyze a different approach based on iterative methods, which are often preferred in inverse problems thanks to their good regularization capabilities.

By considering again the linear system $\tilde{E}\tilde{h} = \tilde{b}$ of (3.2), a block splitting decomposition of $\tilde{E}$ gives rise to an effective iterative method whose numerical complexity per iteration is linear with the number of blocks. In particular, starting from an initial guess $\tilde{h}^{(0)}$, due again to the block-arrow structure, each iteration of the simple Jacobi (3.4) and the Gauss-Seidel (3.5) block methods [12] can be written as

$$\begin{bmatrix} \tilde{M}_1 & & & & \\ & \tilde{M}_2 & & & \\ & & \ddots & & \\ & & & \tilde{M}_P & \\ & & & & \tilde{C} \end{bmatrix} \tilde{h}^{(t+1)} = \tilde{b} - \begin{bmatrix} & & & & V_1 \\ & & & & V_2 \\ & & & & \vdots \\ & & & & V_P \\ V_1^* & V_2^* & \dots & V_P^* & 0 \end{bmatrix} \tilde{h}^{(t)} \tag{3.4}$$

and

$$\begin{bmatrix} \tilde{M}_1 & & & & \\ & \tilde{M}_2 & & & \\ & & \ddots & & \\ & & & \tilde{M}_P & \\ V_1^* & V_2^* & \dots & V_P^* & \tilde{C} \end{bmatrix} \tilde{h}^{(t+1)} = \tilde{b} - \begin{bmatrix} & & & & V_1 \\ & & & & V_2 \\ & & & & \vdots \\ & & & & V_P \\ & & & & 0 \end{bmatrix} \tilde{h}^{(t)}, \tag{3.5}$$

respectively.

Let $\tilde{b} = \left(b_1, b_2, \dots, b_P, b_\chi\right)^T$ and $\tilde{h} = \left(h_1, h_2, \dots, h_P, h_\chi\right)^T$ denote again the block form of the right-hand side and of the solution of (3.2), and partition the iterates $\tilde{h}^{(t)}$ accordingly. Exploiting the simple inverse of triangular arrow (block) matrices, we can summarize the two splitting methods as follows:

$$h_p^{(t+1)} = \tilde{M}_p^{-1}\left(b_p - V_p^* h_\chi^{(t)}\right), \tag{3.6}$$

for $p = 1, \dots, P$, and

$$h_\chi^{(t+1)} = \tilde{C}^{-1}\left(b_\chi - \sum_{p=1}^{P} V_p^* q_p^{(t)}\right), \tag{3.7}$$

where $q_p^{(t)} = h_p^{(t)}$ for the Jacobi iteration (3.4) and $q_p^{(t)} = h_p^{(t+1)}$ for the Gauss-Seidel iteration (3.5).

Provided that $V_p \neq 0$ for all p (otherwise we would obtain a further simplification by uncoupling some equations), it is straightforward to verify that block-arrow matrices are 2-cyclic and consistently ordered according to the classical definitions of Varga [27]; as an interesting consequence, the convergence rate of the block Gauss-Seidel method is twice the convergence rate of the block Jacobi one. Indeed, it can be proved that

$$\rho(B_G) = (\rho(B_J))^2,$$

where $\rho(B_G)$ is the spectral radius of the Gauss-Seidel iteration matrix

$$B_G = \begin{bmatrix} \tilde{M}_1 & & & & \\ & \tilde{M}_2 & & & \\ & & \ddots & & \\ & & & \tilde{M}_P & \\ & & & & \tilde{C} \end{bmatrix}^{-1} \begin{bmatrix} & & & & V_1 \\ & & & & V_2 \\ & & & & \vdots \\ & & & & V_P \\ V_1^* & V_2^* & \dots & V_P^* & 0 \end{bmatrix},$$

ETNA
Kent State University
http://etna.math.kent.edu

and $\rho(B_J)$ is the spectral radius of the Jacobi iteration matrix

$$B_J = \begin{bmatrix} \tilde{M}_1 & & & & \\ & \tilde{M}_2 & & & \\ & & \ddots & & \\ & & & \tilde{M}_P & \\ V_1^* & V_2^* & \dots & V_P^* & \tilde{C} \end{bmatrix}^{-1} \begin{bmatrix} & & & & V_1 \\ & & & & V_2 \\ & & & & \vdots \\ & & & & V_P \\ & & & & 0 \end{bmatrix}.$$

On the other hand, the Jacobi method, although slower, can be implemented fully in parallel, where any one of the $P+1$ block systems given by (3.6) and (3.7) can be solved independently on a different processor. The same trick for the Gauss-Seidel method would require about double the computation time, since the computation of (3.7) must follow the computation of the P independent block systems (3.6), for $p = 1, \dots, P$.

Every step of such iterative methods involves the solution of the inner linear systems (3.6) and (3.7) at the block level only (notice that the matrix inverses are $\tilde{M}_p^{-1}$, for $p = 1, \dots, P$, and $\tilde{C}^{-1}$, all of them $n^2 \times n^2$ matrices), which can be solved either by inner direct or by inner iterative methods. In the latter case, the regularization capabilities of iterative methods can be very favorable, since early termination of the iterations leads to a regularized solution of the system. With this choice, it is possible to solve the (unregularized) system with coefficient matrix (3.1) instead of the Tikhonov regularized one (3.2), since now regularization is enforced in the innermost iterative method. In particular, as we will see in the next subsection, this is the choice we adopt in the proposed solution method and use for the numerical tests.

3.2. A three-level inexact-Newton Method. The inexact-Newton algorithm we propose is an iterative regularizing method for nonlinear equations, where each linearized step is regularized by means of an iterative regularization scheme based on a block splitting. The method is useful for all the nonlinear functional equations whose linearization leads to block matrices, as is the case for our model (2.6) with linearization (2.9).

The method can be introduced as follows, where, for the sake of simplicity, we explicitly refer to the model (2.6).

1. Set $k = 0$. Choose the initial guess $x_0 = (u_{1,0}, \dots, u_{P,0}, \chi_0)$, where:
   - χ_0 is an approximation of the target distribution χ. If no information is available, set $\chi_0 = 0$.
   - $u_{p,0} = u_p^i$, for $p = 1, \dots, P$ (notice that the initial guess of the unknown total fields are simply initialized to be the known incident field; this is the basic choice of the widely used first order Born approximation scheme for inverse scattering [7]).
2. Linearize equation (2.6) at the point $x_k = (u_{1,k}, \dots, u_{P,k}, \chi_k)$ by means of the Fréchet derivative A'_{x_k} of the operator A, as shown in (2.9), obtaining the Gauss-Newton linear equation
$$A'^*_{x_k} A'_{x_k} h_k = A'^*_{x_k}(b - A(x_k)), \tag{3.8}$$
   where $h_k = (h_{k,1}, \dots, h_{k,P}, h_{k,\chi})$ and $A'^*_{x_k}(b - A(x_k)) = (b_{k,1}, \dots, b_{k,P}, b_{k,\chi})$.
3. Consider the block splitting methods (3.4) or (3.5) without Tikhonov regularization (i.e., with $\mu = 0$) for the solution of equation (3.8).
   Set $\widetilde{h}_{k,p}^{(0)} = 0$ and $\widetilde{h}_{k,\chi}^{(0)} = 0$. For $t = 0, 1, 2, \dots, T(k)$:
   (i) Compute a regularized solution $\widetilde{h}_{k,p}^{(t+1)}$, $p = 1, \dots, P$, of the first P diagonal system blocks
$$M_p h_{k,p}^{(t+1)} = b_{k,p} - V_p^* \widetilde{h}_{k,\chi}^{(t)} \tag{3.9}$$

ETNA
Kent State University
http://etna.math.kent.edu

by means of a fixed number $K_1 = K_1(k,t,p)$ of iterations of the Landweber regularization iterative method for linear systems (or another iterative regularization method). For the Landweber method applied to the pth equation, setting $f_0 = 0$, we have

$$f_{s+1} = f_s + \tau M_p^*(b_{k,p} - V_p^* \widetilde{h}_{k,\chi}^{(t)} - M_p f_s), \tag{3.10}$$

where $\tau = 1/\|M_p\|_2$ is a fixed convergence parameter, chosen according to the discussion of Section 2.2, and M_p is the system matrix. Hence, the regularized solution is $\widetilde{h}_{k,p}^{(t+1)} = f_{K_1}$.

(ii) Compute a regularized solution $\widetilde{h}_{k,\chi}^{(t+1)}$ of the last row system block

$$C h_{k,\chi}^{(t+1)} = b_{k,\chi} - \sum_{p=1}^{P} V_p^* q_{k,p}^{(t)}, \tag{3.11}$$

where $q_{k,p}^{(t)} = \widetilde{h}_{k,p}^{(t)}$ for the Jacobi iteration (3.4) and $q_{k,p}^{(t)} = \widetilde{h}_{k,p}^{(t+1)}$ for the Gauss-Seidel iteration (3.5), by means of a fixed number $K_2 = K_2(k,t,\chi)$ of iterations of the Landweber iterative regularization method for linear systems (or another iterative regularization method). For the Landweber method, setting $f_0 = 0$, we have

$$f_{s+1} = f_s + \tau C^*(b_{k,\chi} - \sum_{p=1}^{P} V_p^* q_{k,p}^{(t)} - C f_s), \tag{3.12}$$

where $\tau = 1/\|C\|_2$ is a fixed convergence parameter, chosen again according to the discussion of Section 2.2, being C the system matrix. Hence, the regularized solution is $\widetilde{h}_{k,\chi}^{(t+1)} = f_{K_2}$.

4. Setting $\widetilde{h}_k = \left(\widetilde{h}_{k,1}^{(T(k)+1)}, \ldots, \widetilde{h}_{k,P}^{(T(k)+1)}, \widetilde{h}_{k,\chi}^{(T(k)+1)}\right)$, update the solution by

$$x_{k+1} = x_k + \widetilde{h}_k. \tag{3.13}$$

5. Check a stopping rule for x_{k+1}: if it is satisfied, terminate; otherwise set $k \leftarrow k+1$ and go to step 2.

The proposed algorithm can be summarized as a three-level iterative method:

Level I. The outer level of iterations is related to the Gauss-Newton method (3.8), and the iterations are related to the index k. The stopping rule can be the discrepancy principle [23], based on the knowledge of the amount of noise in the data.

Level II. The first inner level of iterations is related to the block splitting, either (3.4) or (3.5), and the iterations are related to the index t as shown by (3.9) and (3.11). A suitable number of iterations $T(k)$ can be estimated by means of preliminary numerical tests and then fixed.

Level III. The second and nested inner level of iterations is related to the computation of (small) numbers K_1 and K_2 of steps of an iterative regularization method, such as Landweber, for each system block (3.9) and (3.11) of *(i)* and *(ii)*. These iterations are related to the index k as shown by (3.10) and (3.12), and the values K_1 and K_2 can be estimated by numerical tests. We notice that, usually, these numbers are small since, due to the severe ill-posedness of the problem, the regularization effects of the inner iterative method have to be high.

ETNA
Kent State University
http://etna.math.kent.edu

The overall cost of each outer iteration is $T(k)+1$ times the operations required by the following $n \times n$ matrix-vector products:

- 2 products involving each V_p, for $p = 1, \dots, P$;
- $2K_1$ products involving each M_p, for $p = 1, \dots, P$;
- $2K_1$ products involving C.

A comparison with the computational cost of the Cholesky direct method of Section 3.1.1 shows that the iterative approach is cheaper when $T(k)$ and K_1 are small compared to n. Of course, the inner structure of the blocks can be helpful to save further computations; this issue will be discussed in Section 3.3.

It is interesting to notice that some other approaches appearing in the literature [23] correspond to a very simplified choice of the parameters of the above scheme. More precisely, the two-level Gauss-Newton method with Landweber inner regularization described in [4] is equivalent to the three-level scheme obtained by setting $K_1 = K_2 = 1$.

3.3. Exploiting the inner structure of the Fréchet derivative. As already noted, A'_x is a sparse and block structured matrix. Moreover, every block of A'_x is given by the discretization of a particular linear operator of the type $B\,h(r) = \int_\Omega s(r,\tilde{r})\,h(\tilde{r})\,d\tilde{r}$, where the integral kernel s is known and is given by the product of the shift invariant kernel G times a fixed function (either χ or u^p, $p = 1, \dots, P$). If each observation domain $\Omega_p^{(M)}$ were equal to the rectangular $n \times n$ investigation domain Ω, then the discretization of all of these integrals would lead to Toeplitz-times-diagonal blocks, whose matrix-vector products cost $O(n^2 \log n)$ by using a fast trigonometric transform, such as the classical FFT (or, better, a different trigonometric transform related to a particular choice of the boundary conditions, such as reflective or antireflective [25]). Unfortunately this does not happen in real applications, since $\Omega_p^{(M)}$ is disjoint (and far) from Ω. Then, although the $n^2 \times n^2$ blocks A_χ and $A_{u,p}$, $p = 1, \dots, P$, of A'_x are always Toeplitz-times-diagonal so that the 2D FFT can be used for the related matrix-vector product, in real applications each $m \times n^2$ block $A_{\chi,p}^{(M)}$ and $A_{u,p}^{(M)}$, $p = 1, \dots, P$, is a small lower rank extracted matrix (that is, a principal submatrix [24]) of a full Toeplitz-times-diagonal matrix. If we consider a larger rectangular discretized $q \times q$ domain Ω_{ext} which contains both the $n \times n$ investigation domain Ω and all the m detectors of each observation domain $\Omega_p^{(M)}$, $p = 1, \dots, P$, then every block $A_{\chi,p}^{(M)}$ can be embedded in a larger $q^2 \times q^2$ Toeplitz-times-diagonal matrix Q_χ, which is associated with the integral operator

$$Q_\chi h(r) = \int_{\Omega_{ext}} G(r,\tilde{r})\,h(\tilde{r})\,\chi(\tilde{r})\,d\tilde{r}$$

for any $r \in \Omega_{ext}$. In this way, it is possible to factorize $A_{\chi,p}^{(M)}$ as

$$A_{\chi,p}^{(M)} = R_p^{(M)} Q_\chi T,$$

where the matrix $R_p^{(M)}$ is a $m \times q^2$ restriction matrix from Ω_{ext} to $\Omega_p^{(M)}$ and the matrix T is a $q^2 \times n^2$ canonical injection from Ω to Ω_{ext} (similarly for $A_{u,p}^{(M)}$). According to this trick, the matrix-vector product for any block $A_{\chi,p}^{(M)}$ and $A_{u,p}^{(M)}$ costs $O(q^2 \log q)$ instead of $O(mn^2)$.

In practice, the appropriate computation procedure for all the $A_{\chi,p}^{(M)}$ and $A_{u,p}^{(M)}$ matrix-vector products depends on both *(i)* the number and the position of the detectors of $\Omega_p^{(M)}$ and *(ii)* the dimension and the discretization step of Ω. Suppose, for example, that Ω_{ext} is k times larger than Ω, so that $q = kn$, and assume that a $q \times q$ 2D FFT requires $8q^2 \log q$ multiplications; see [28] for the 1-D FFT. Then the matrix-vector product with Q_χ is cheaper than the matrix-vector product with $A^{(M)}_{\chi,p}$ when $3 \cdot 8 \cdot k^2 n^2(\log(k) + \log(n)) < mn^2$ (the factor 3 is given by the fact that a matrix product involves two forward FFTs and one inverse FFT, and we ignore the contribution of the n^2 pointwise matrix product). That is, the approach using Q_χ is cheaper when

$$24k^2(\log(k) + \log(n)) < m.$$

In real applications, the number m of detectors is about two to three hundred, and so the FFT is not useful for small k and small discretization parameters n. In the simplified case where the detectors are equispaced on the perimeter of the rectangular domain Ω_{ext}, with the same step size of Ω, we have that $m = 4kn$, so that the previous inequality becomes

$$6k(\log(k) + \log(n)) < n.$$

In this case, with $n = 1024$, the matrix-vector products using 2D FFTs is better for $k < 13$; with $n = 256$, for $k < 5$; and with $n = 35$, as in our numerical tests, for $k < 2$. This shows that, at least in our configuration where the investigation domain is much smaller and far from the measurement one, the FFT does not reduce the computational complexity of matrix-vector products for all the blocks $A^{(M)}_{\chi,p}$ and $A^{(M)}_{u,p}$, $p = 1, \ldots, P$.

We mention that a similar idea of embedding the discretization points of a general domain into a larger rectangular domain in order to obtain a (block) Toeplitz matrix was also used in [26] to describe the spectral properties of a class of structured matrices; the related information also could be important for tuning appropriate regularizing methods.

3.4. Post-processing enhancement by super-resolution techniques. A significant difficulty in microwave imaging is that the reconstructed images have fairly low resolution. To obtain higher resolution images we consider a post processing technique called *super-resolution*, which is essentially an example of data fusion; see, for example, [3, 6, 11, 21]. The aim is to reconstruct a high resolution image from a set of known low resolution images, each shifted by subpixel displacements. In our application we reconstruct r images, each reconstructed independently by shifting slightly the microwave tomographic apparatus. Let $\chi_1, \chi_2, \ldots, \chi_r$ be the reconstructed low resolution images (e.g., using the previously described three-level inexact Newton method). It is assumed that each low resolution image is shifted by subpixel displacements from a particular reference image. These subpixel displacements suggest that each low resolution image contains different information about the same object. The aim is to fuse this different information into one high resolution image. To describe the mathematical model of super-resolution, we assume each low resolution image can be represented as

$$\chi_j = DS(y_j)\chi + \eta_j, \quad j = 1, \ldots, r,$$

where η_j is additive noise, D is a decimation matrix that transforms a high resolution image into a low resolution image, and S is a sparse matrix that performs a geometric distortion (e.g., shift) of the high resolution image, χ. The geometric distortion, and hence S, is defined by the parameter vector y_j. The reconstruction problem amounts to computing χ from the inverse problem

$$\begin{bmatrix} \chi_1 \\ \chi_2 \\ \vdots \\ \chi_r \end{bmatrix} = \begin{bmatrix} DS(y_1) \\ DS(y_2) \\ \vdots \\ DS(y_r) \end{bmatrix} \chi + \begin{bmatrix} \eta_1 \\ \eta_2 \\ \vdots \\ \eta_r \end{bmatrix}. \tag{3.14}$$

ETNA
Kent State University
http://etna.math.kent.edu

Note that if we assume that each of the low resolution images are shifted horizontally and vertically, then each y_j contains only two values (the horizontal and vertical displacements). If we want to consider more complicated movements (such as rotation), then each y_j might contain up to six values that define general linear affine transformations. In either case, clearly there are significantly fewer parameters defining $y_1, \ldots, y_r$ than the number of pixel values defining χ.

In many cases, the parameters y_j can be accurately determined from the imaging system; that is, the subpixel shifts can be measured during a calibration process. In this case, equation (3.14) is a linear inverse problem, and standard techniques such as conjugate gradients with Tikhonov regularization can be used to compute an approximation of χ. However, if the parameter vector y_j is not known, then an optimization scheme must be used to jointly estimate χ and y_j. In this case, since there are relatively few parameters defining y_j, an efficient separable nonlinear least squares approach can be used; see [6].

4. Numerical Experiments. In this section, a first implementation of the proposed method has been developed and tested on two different scatterers to provide some numerical results. A set of low resolution reconstructions related to the microwave imaging model (2.6) in a tomographic configuration are computed by the algorithm of Section 3.2 on several data sets related to subpixel linear shifts of the apparatus. After that, the super-resolution enhancement technique of Section 3.4 is applied in order to improve the accuracy.

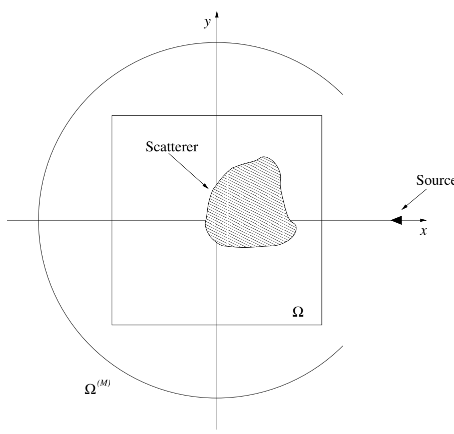

FIGURE 4.1. *Microwave tomographic apparatus*

The tomographic arrangement is shown in Figure 4.1 and can be summarized as follows:

- the scattering object under test is contained in a square investigation area Ω centered at the origin, whose edge is 1m (meter) for the first test, 0.8m for the second one, and the (low resolution) discretization size is $n \times n = 31 \times 31$;
- there are $m = 241$ receiving antennas equispaced on an arc of $\frac{4\pi}{3}$ radians belonging to a circumference centered at the origin, whose diameter is 3.34m;
- the number of rotations of the whole tomographic apparatus is $R = 8$, each one equispaced by $\frac{\pi}{4}$ radians;
- for each rotation, the scattering object is illuminated by a single incident plane microwave, i.e. $F = 1$, with a frequency of 0.3 GHz (wavelength 10^{-3}m) for the first test and 0.8 GHz (wavelength $2.6 \cdot 10^{-3}$m) for the second one.

With this setting, for the jth rotation, the ith receiver is placed at the position $(\rho, \theta) = (1.67, (j-1)\frac{\pi}{4} + \frac{\pi}{3} + \frac{i-1}{m-1}\frac{4\pi}{3})$, in polar coordinates, for $i = 1, \ldots, m$ and $j = 1, \ldots, R$.

ETNA
Kent State University
http://etna.math.kent.edu

The total field u measured by the receiving antennas is characterized by a signal-to-noise ratio (SNR) of 25 dB; that is, the relative noise on the measured scattered fields is about 0.6%.

In this first implementation of the proposed three-level algorithm, we use the block Jacobi splitting (3.4) and the Landweber method for the innermost block level, as shown by the schemes (3.10) and (3.12). It is important to remark that for all the simulations the whole algorithm is initialized by an empty scene, i.e., for the initial guess $x_0 = (u_{1,0}, \ldots, u_{P,0}, \chi_0)$ we simply set $\chi_0 = 0$ (as if no scatter were involved) and $u_{p,0} = u_p^i$, $p = 1, \ldots, P$ (as if no scattered field were produced). In this way, in our tests no *a priori* information is used and needed.

The three-level algorithm requires the choice of *(i)* the number of outer Newton iterations related to the index k of (3.8), *(ii)* the number $T(k)$ of block splitting iterations, related to the index t of (3.9) and (3.11), for any Newton iteration k, and *(iii)* the numbers $K_1(k, t, p)$ and $K_2(k, t, \chi)$ of Landweber iterations respectively related to the index s of Landweber iterations (3.10) and (3.12), for any Newton iteration k, any splitting iteration t, and any incident wave p.

In real applications, the outer Newton iterations (3.8) can be stopped by means of a discrepancy principle rule very similar to the classical one used for linear inverse problems [2]. That is, the iteration is terminated as soon as $\|A(x_k) - b\| \le \tau\eta$, where $\tau > 1$ is an experimentally estimated small constant and η is an estimate of the noise in the data b; see [23] for details about the discrepancy principle for nonlinear inverse problems. In these preliminary tests with simulated data, we stop the Newton method after 30 iterations, a number that was chosen experimentally by comparing the output of several different tests. The number of block Jacobi iterations $T(k)$ is fixed equal to 10, and the number of inner Landweber iterations is $K_1(k, t, p) = K_2(k, t, \chi) = 1$.

For the computation of the right-hand side of (3.8), the investigation domain Ω is partitioned into 35×35 square subdomains, and the forward operator A is computed by applying the method of moments with pulse-basis functions and point matching to every instance of the equations (2.2) and (2.3), as explained at the end of Section 2.2.

After the restorations provided by the three-level algorithm, the super-resolution technique has been applied. The super-resolution leads to a large-scale ill-posed linear problem which requires a regularization algorithm. In our implementation, this linear problem is solved by a small number of projected Landweber iterations [5], starting with an initial guess which is the low resolution restoration in the basic center position. Specifically, five low resolution (LR) images from the three-level algorithm for microwave inverse scattering are the input data that allow us to retrieve the one high resolution (HR) output image. The five LR images are the reference image at the center of the coordinates and the four images shifted by $1/3$ of a pixel respectively to the right, to the left, to the top, and to the bottom. With this enhancement technique, we obtain 62×62 images from 31×31 microwave restorations, with a reduction of the restoration error which is often larger than 10%.

The relative restoration error of the output image χ of the scatterer is evaluated by computing $\|\widetilde{\chi} - \chi\|_F / \|\widetilde{\chi}\|_F$ where $\widetilde{\chi}$ is the known true configuration of the scatterer, and $\|\cdot\|_F$ is the Frobenius norm of matrices. In the figures, the plots show the values of the relative refractive index $\epsilon(r)/\epsilon_b = \chi(r) + 1$, as described in Section 2.1.

Test 1. The first test concerns the reconstruction of a homogeneous scatterer satisfying the hypotheses of Section 2, whose shape is similar to the digit "eight" and is shown in Figure 4.2 (top left). The boundary of the scatterer has the parametric form given by formulas

$$x(t) = \sqrt{\cos^2(t) + 8\sin^2(t)}\,\cos(t)/6.6 \quad \text{and} \quad y(t) = \sqrt{\cos^2(t) + 8\sin^2(t)}\,\sin(t)/6.6,$$

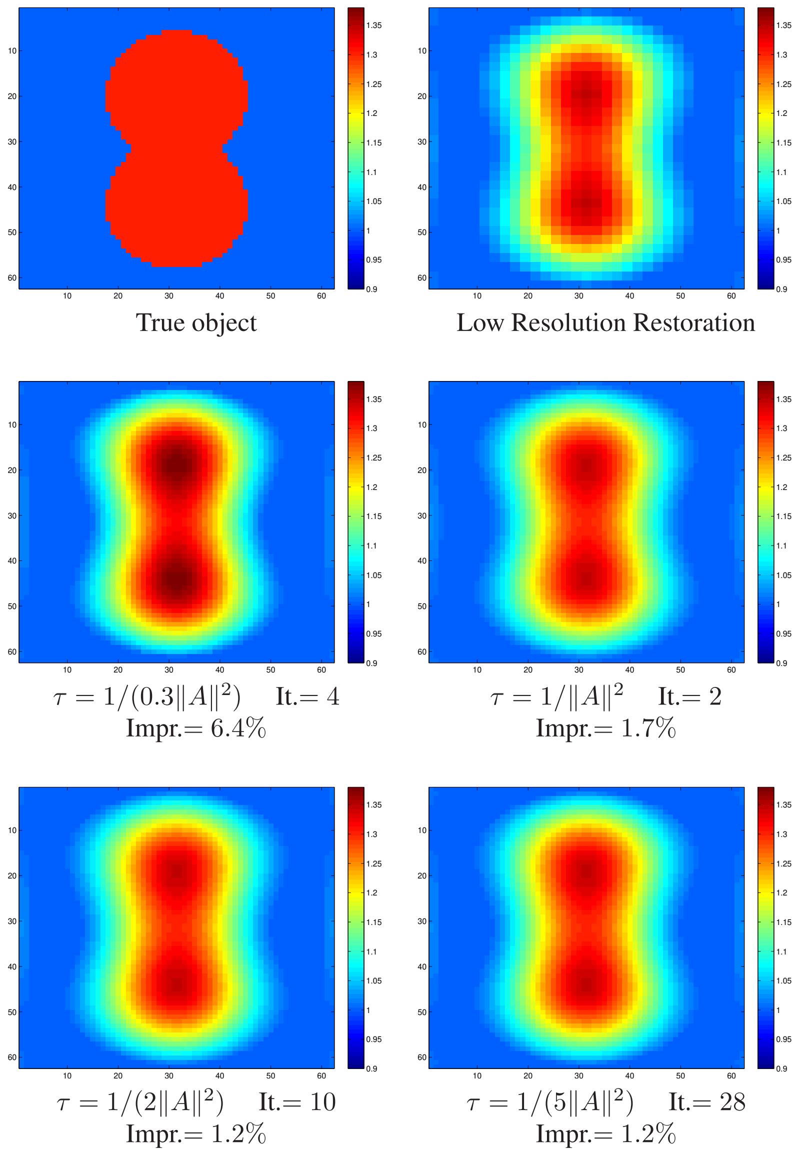

FIGURE 4.2. *Test 1 – True object and best reconstructions.*

with $t \in [0, 2\pi]$, and with a 1m square investigation domain. The contrast function $\widetilde{\chi}$ of the scatterer is constant and equal to 0.3. The LR reference image of the contrast function is shown in Figure 4.2 (top right); some HR reconstructed distributions of the contrast function are reported in Figure 4.2 (second and third row) for different values of the convergence parameter τ of the projected Landweber method used in the super-resolution step (recall the discussion of the role of τ in Section 2.2). For each HR image, we show the number of projected Landweber iterations and the improvement between the LR and HR restorations, that is, the difference between the relative restoration error of the LR image and the relative restoration error of the HR image.

Figure 4.3 shows the pointwise difference between the true and the reconstructed objects.

ETNA
Kent State University
http://etna.math.kent.edu

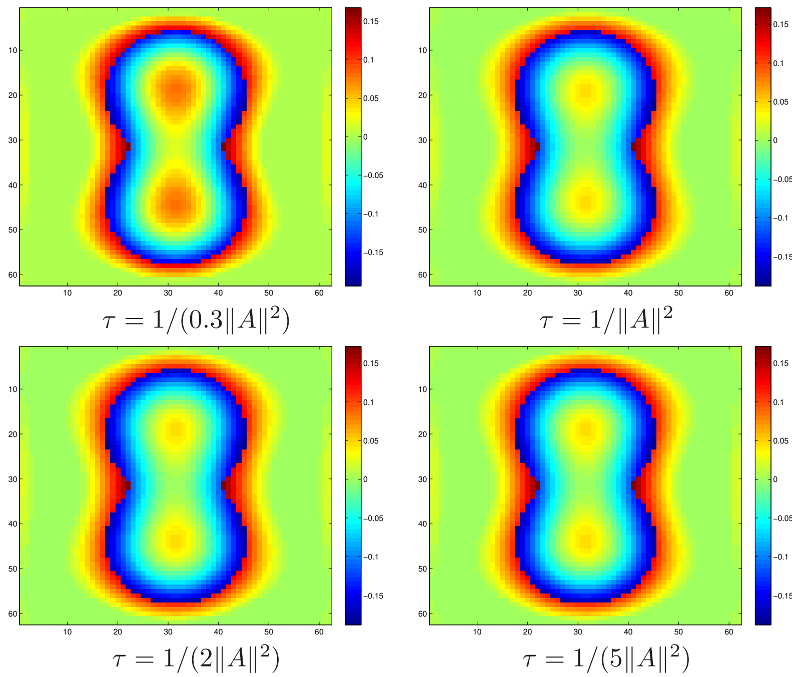

FIGURE 4.3. *Test 1 – Absolute restoration errors.*

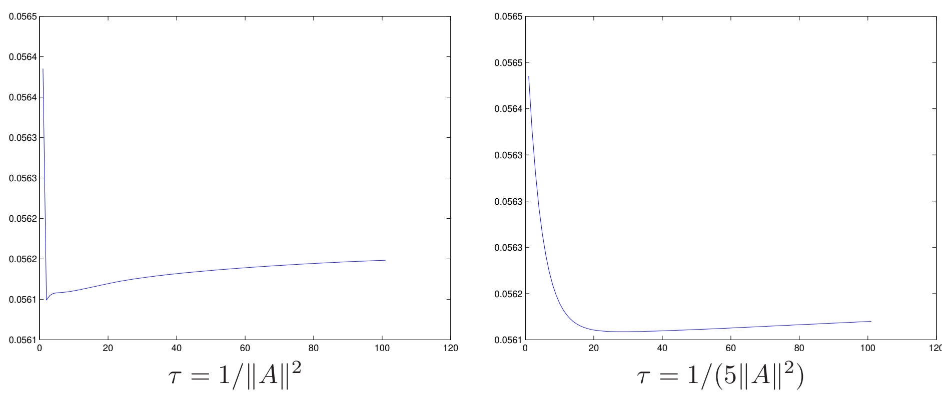

FIGURE 4.4. *Test 1 – Super-resolution convergence history.*

These restoration error results show that the localization of the object and the reconstruction of the permittivity are good, although the edges are smoothed due to the regularization effects of the algorithm.

The convergence history of the projected Landweber method for the super-resolution technique, illustrated by a plot of the relative restoration error versus the iteration number, is shown in Figure 4.4.

Test 2. The second simulation is related to a circular homogeneous annulus centered at the origin, with external diameter of 0.4m and internal diameter of 0.2m, and two smaller homogeneous disks with diameter of 0.1m centered at $(-0.25\text{m}, 0.25\text{m})$ and $(0.25\text{m}, 0.25\text{m})$, where the size of the square investigation domain is 0.8m. This configuration with a hole can

ETNA
Kent State University
http://etna.math.kent.edu

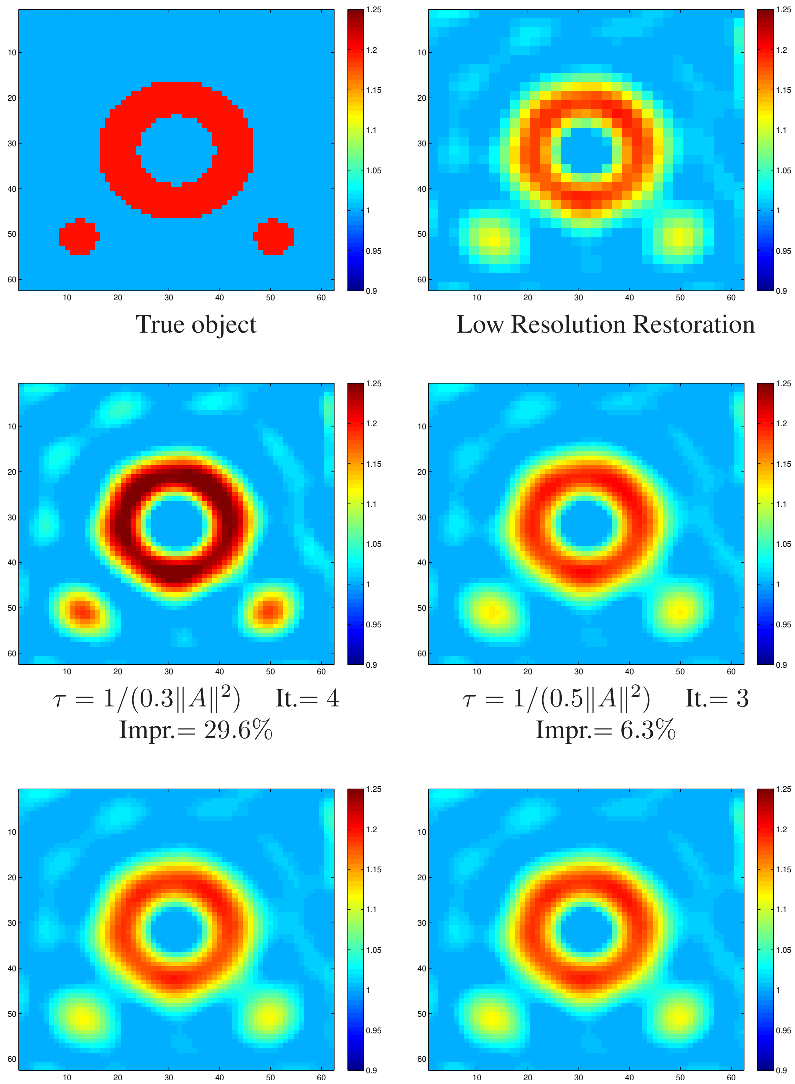

True object — Low Resolution Restoration

$\tau = 1/(0.3\|A\|^2)$ It.$= 4$ Impr.$= 29.6\%$ — $\tau = 1/(0.5\|A\|^2)$ It.$= 3$ Impr.$= 6.3\%$

$\tau = 1/\|A\|^2$ It.$= 9$ Impr.$= 2.1\%$ — $\tau = 1/(5\|A\|^2)$ It.$= 25$ Impr.$= 2.1\%$

FIGURE 4.5. *Test 2 – True object and best reconstructions.*

be of interest for nondestructive evaluation purposes in civil engineering.

The contrast function $\widetilde{\chi}$ of the scatterer is constant and equal to 0.3. As in Test 1, the LR reference image of the contrast function is shown in Figure 4.5 (top right) and some HR reconstructed distributions of the contrast function are reported in Figure 4.5 (second and third row) for different values of the convergence parameter τ of the projected Landweber method used in the super-resolution step. Figure 4.6 shows the pointwise restoration errors, and the convergence history for the super-resolution technique is shown in Figure 4.7.

For small values of τ, the convergence is slow and more regular (see the images on the third row of Figure 4.5); whereas for larger values of τ, the convergence is faster and the restorations are better, but it is much more difficult to stop the Landweber iteration for the

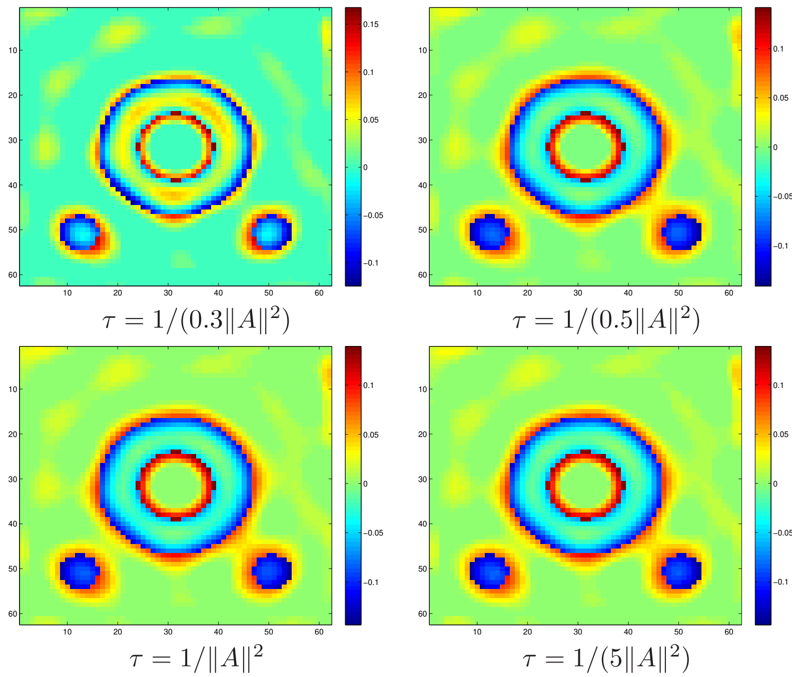

FIGURE 4.6. *Test 2 – Absolute restoration errors.*

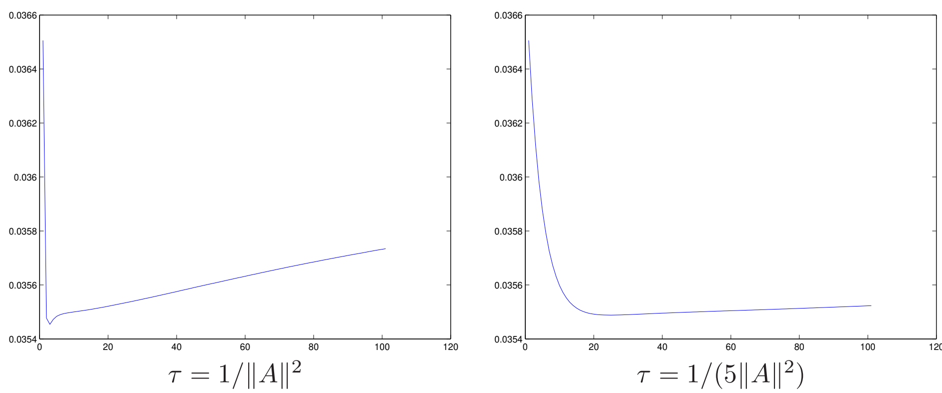

FIGURE 4.7. *Test 2 – Super-resolution convergence history.*

super-resolution technique (see the images on the second row of Figure 4.5 and the convergence histories of Figure 4.7). As can be seen, the localization of the objects in the HR restoration is good and much better than in the LR image. We remark that, from a qualitative point of view, the improvement is much more evident than the percentage quantities would show. In addition, although the estimate of the values of contrast χ is quite satisfying, the shape of the scatterer is not estimated very accurately because of the severe ill-posedness of the problem and the required regularization.

Acknowledgements. The authors would like to thank G. Bozza and A. Randazzo from the Department of Biophysical and Electronic Engineering (DIBE) at the University of Genova, who have provided some of the numerical results used in this paper.

REFERENCES

[1] K. BELKEBIR AND M. SAILLARD, *Testing inversion algorithms against experimental data: inhomogeneous targets*, Inverse Problems, 21 (2004), pp. S1–S3.

[2] M. BERTERO AND P. BOCCACCI, *Introduction to Inverse Problems in Imaging*, Institute of Physics Publishing, Bristol, 1998.

[3] N. K. BOSE AND K. J. BOO, *High-resolution image reconstruction with multisensors*, Int. J. Imaging Syst. Technol., 9 (1998), pp. 294–304.

[4] G. BOZZA, C. ESTATICO, M. PASTORINO, AND A. RANDAZZO, *An inexact Newton method for microwave reconstruction of strong scatterers*, IEEE Antennas and Wireless Propag. Lett., 5 (2006), pp. 51–54.

[5] P. BRIANZI, F. DI BENEDETTO, AND C. ESTATICO, *Improvement of space-invariant image deblurring by preconditioned Landweber iterations*, SIAM J. Sci. Comp., 30 (2008), pp. 1430–1458.

[6] J. M. CHUNG, E. HABER, AND J. G. NAGY, *Numerical methods for coupled super-resolution*, Inverse Problems, 22 (2006), pp. 1261–1272.

[7] D. COLTON AND R. KRESS, *Inverse Acoustic and Electromagnetic Scattering Theory*, second ed., Springer, Berlin, 1998.

[8] M. ELAD AND A. FEUER, *Restoration of a single superresolution image from several blurred, noisy, and undersampled measured images*, IEEE Trans. Image Process., 6 (1997), pp. 1646–1658.

[9] H. W. ENGL, M. HANKE, AND A. NEUBAUER, *Regularization of Inverse Problems*, Kluwer Academic Press, Dordrecht, 1996.

[10] H. W. ENGL AND P. KUGLER, *Nonlinear inverse problems: theoretical aspects and some industrial applications*, in Multidisciplinary Methods for Analysis, Optimization and Control of Complex Systems, Mathematics in Industry, 6, Springer, Berlin, 2004, pp. 3–48.

[11] S. FARSIU, D. ROBINSON, M. ELAD, AND P. MILANFAR, *Advances and challenges in super-resolution*, Int. J. Imaging Syst. Technol., 14 (2004), pp. 47–57.

[12] G. H. GOLUB AND C. F. VAN LOAN, *Matrix Computations*, third ed., The Johns Hopkins University Press, London, 1996.

[13] M. HANKE, *Accelerated Landweber iterations for the solutions of ill-posed problems*, Numer. Math., 60 (1991), pp. 341–373.

[14] M. HANKE, A. NEUBAUER, AND O. SCHERZER, *A convergence analysis of Landweber iteration for nonlinear ill-posed problems*, Numer. Math., 72 (1995), pp. 21–37.

[15] F. HARRINGTON, *Field Computation by Moment Methods*, Macmillan, New York, 1968.

[16] T. HOHAGE, *On the numerical solution of a 3D inverse medium scattering problem*, Inverse Problems, 17 (2001), pp. 1743–1763.

[17] M. G. KANG AND S. CHAUDHURI, *Super-resolution image reconstruction*, IEEE Signal Processing Magazine, 20 (2003), pp. 19–20.

[18] A. KIRSCH, *An Introduction to the Mathematical Theory of Inverse Problems*, Springer, New York, 1996.

[19] N. NGUYEN, P. MILANFAR, AND G. GOLUB, *A computationally efficient superresolution image reconstruction algorithm*, IEEE Trans. Image Process., 10 (2001), pp. 573–583.

[20] M. PASTORINO, *Recent inversion procedures for microwave imaging in biomedical, subsurface detection and nondestructive evaluation*, Measurement, 36 (2004), pp. 257–269.

[21] S. PRASAD, *Digital supereresolution and the generalized sampling theorem*, J. Opt. Soc. Amer. A, 24 (2007).

[22] J. H. RICHMOND, *Scattering by a dielectric cylinder of arbitrary cross section shape*, IEEE Trans. Antennas Propagat., 13 (1965), pp. 334–341.

[23] A. RIEDER, *On the regularization of nonlinear ill-posed problems via inexact Newton iterations*, Inverse Problems, 15 (1999), pp. 309–327.

[24] S. SALAPAKA AND A. PIERCE, *Analysis of a novel preconditioner for a class of p-level lower rank extracted systems*, Numer. Linear Algebra Appl., 12 (2006), pp. 437–472.

[25] S. SERRA-CAPIZZANO, *A note on antireflective boundary conditions and fast deblurring methods*, SIAM J. Sci. Comp., 25 (2004), pp. 1307–1325.

[26] ———, *GLT sequences as a generalized Fourier analysis and applications*, Linear Algebra Appl., 419 (2006), pp. 180–233.

[27] R. S. VARGA, *Matrix Iterative Analysis*, second ed., Springer, Berlin, 2000.

[28] R. YAVNE, *An economical method for calculating the discrete Fourier transform*, in Proc. AFIPS Fall Joint Computer Conf., ACM, New York, 1968, pp. 115–125.